Nanocube Superlattices of Cesium Lead Bromide Perovskites and Pressure-Induced Phase Transformations at Atomic and Mesoscale Levels

*Yasutaka Nagaoka, Katie Hills-Kimball, Rui Tan, Ruipeng Li, Zhongwu Wang, and Ou Chen**

Lead halide perovskites are promising materials for a range of applications owing to their unique crystal structure and optoelectronic properties. Understanding the relationship between the atomic/mesostructures and the associated properties of perovskite materials is crucial to their application performances. Herein, the detailed pressure processing of $CsPbBr_3$ perovskite nanocube superlattices (NC-SLs) is reported for the first time. By using in situ synchrotron-based small/wide angle X-ray scattering and photoluminescence (PL) probes, the NC-SL structural transformations are correlated at both atomic and mesoscale levels with the band-gap evolution through a pressure cycle of 0 ↔ 17.5 GPa. After the pressurization, the individual $CsPbBr_3$ NCs fuse into 2D nanoplatelets (NPLs) with a uniform thickness. The pressure-synthesized perovskite NPLs exhibit a single cubic crystal structure, a 1.6-fold enhanced photoluminescence quantum yield, and a longer emission lifetime than the starting NCs. This study demonstrates that pressure processing can serve as a novel approach for the rapid conversion of lead halide perovskites into structures with enhanced properties.

Lead halide perovskites (i.e., ABX_3, where B = Pb, X = Cl, Br, or I) have unique chemical compositions, crystal structures, and superior optoelectronic properties, and therefore, emerge as pivotal materials in current energy and optical-related studies.[1] Further understanding of the structural details and properties is urgently needed to fulfill the potential of lead halide perovskites in applications.[1a] In this context, a high pressure technique using diamond anvil cells (DACs) coupled with in situ X-ray scattering techniques and characterization tools offers one comprehensive way to investigate the structure–property relationship of materials.[2] For example, Wang et al. reported that the electrical resistance and photocurrent of methylammonium lead bromide ($MAPbBr_3$) perovskites were highly sensitive to the crystal structure change under pressure.[3] Jiang et al. discovered that the band gap alignment of $MAPbI_3$ perovskites can be fine-tuned using pressure.[4a] However, these reported studies have been limited to bulk perovskites without considerations of the perovskite crystals' sizes, shapes, and assemblies.

Herein, we studied, for the first time, the behavior of self-assembled $CsPbBr_3$ perovskite nanocube superlattices (NC-SLs) under high pressure. We derived detailed correlations of the band gaps and atomic/mesoscale structures of $CsPbBr_3$ NC-SLs as functions of pressure. Moreover, we found that pressure converted periodically ordered NCs into lateral 2D nanoplatelets (NPLs) that have essentially identical thicknesses, great crystallinity, and enhanced optical properties. Our results not only suggest that this pressure technique can serve as an efficient approach to access new types of perovskite materials overcoming the limitations of conventional synthetic chemistry, but also sheds light on the rational materials design of perovskites.

$CsPbBr_3$ perovskite NCs were synthesized by modifying a published method (see details in the Supporting Information)[5] **Figure 1**A shows the absorption and photoluminescence (PL) spectra of the NCs we produced. The electronic absorption features and the sharp emission peak (full width at half maximum (FWHM) ≈19 nm) indicated the monodispersity of the sample. Transmission electron microscopy (TEM) measurement confirmed that the NCs were highly uniform with an average edge length of 10.2 ± 0.6 nm (Figure 1B). The typical square pattern of the atomic fringes, with a *d*-spacing of 5.8 Å, indicated the high crystallinity of individual NCs (Figure 1B, inset). The crystal structure of the $CsPbBr_3$ NCs was identified by a high-resolution (HR), synchrotron-based, wide angle X-ray scattering (WAXS) technique, and the coexistence of an orthorhombic phase (a_{or} = 8.230 Å, b_{or} = 11.901 Å, and c_{or} = 8.156 Å) and a cubic phase (a_c = 5.862 Å) was observed (Figure S3, Supporting Information).[6]

Self-assembled NC-SLs were formed upon solvent evaporation of the $CsPbBr_3$ NCs suspension. The resulting SLs

Dr. Y. Nagaoka, K. Hills-Kimball, Dr. R. Tan, Prof. O. Chen
Department of Chemistry
Brown University
324 Brook St. Providence, RI 02912, USA
E-mail: ouchen@brown.edu
Dr. R. Li, Dr. Z. Wang
Cornell High Energy Synchrotron Source
Cornell University
Ithaca, NY 14853, USA

DOI: 10.1002/adma.201606666

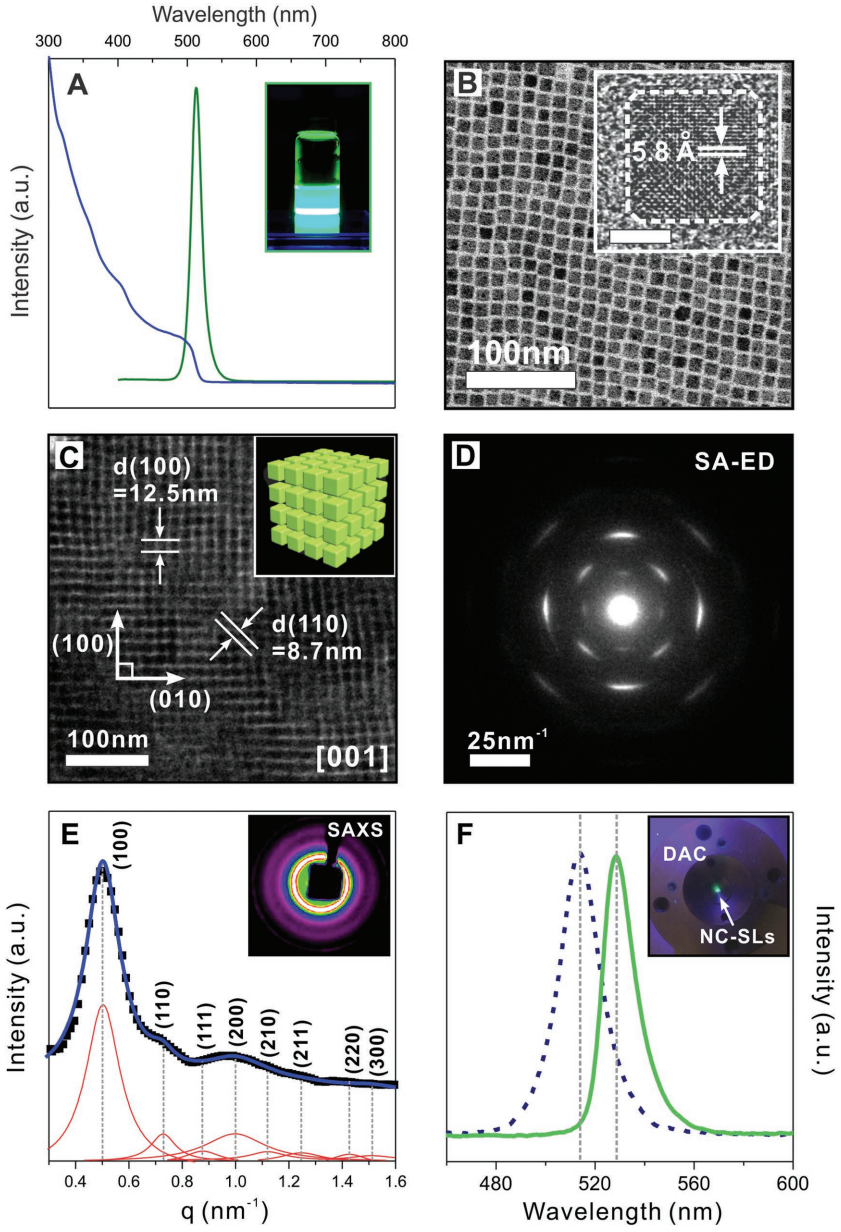

Figure 1. A) Absorption (blue) and PL (green) spectra of the NCs with the inset showing a photograph of the NCs in toluene under UV illumination. B) A typical TEM image of the $CsPbBr_3$ perovskite NCs with an average edge length of ≈10.2 nm with the inset showing a high-resolution TEM image (scale bar, 5 nm). C) A representative TEM image of NC-SLs viewed along the [001] zone axis. D) The corresponding SA-ED pattern. E) SAXS pattern (integrated from the inset image) and the fitted peaks (red), indicative of a simple-cubic packing. F) The PL spectra of the NCs in solutions (blue dotted line) and the assembled NC-SLs (green solid line) with the inset showing a photograph of the NC-SLs emitting inside a DAC under UV illumination.

had a simple cubic superstructure with a lattice constant of ≈12.5 nm (Figures 1C,D and Figure S4, Supporting Information). The small angle X-ray scattering (SAXS) pattern unambiguously confirmed the simple cubic superstructure of the SLs (Figure 1E and Table S3, Supporting Information). The inter-NC separation was determined to be ≈2.3 nm, suggesting the intercalation of surface-coating ligands between neighboring NCs. The SLs emitted a sharp PL emission at 528 nm with an FWHM of ≈15 nm (Figure 1F). This PL peak was ≈15 nm redshifted and ≈25% narrower than the solvent-dispersed NCs, indicating that the densely packed NC-SLs underwent a photon propagation process that resulted in the re-absorption and re-emission of light (Figure 1F).[7]

SAXS, WAXS, and PL spectra were obtained simultaneously from the same compressed volume of NC-SLs.[3,4,8] **Figure 2**A shows a series of WAXS patterns collected from the NC-SLs during a compression cycle of 0 ↔ 17.5 GPa, during which four pressure-induced atomic structural phases were identified (Figure S5, Supporting Information). The $CsPbBr_3$ NCs were originally comprised of a mixture of cubic and orthorhombic phases (Stage I, Figure S3, Supporting Information). These phases merged into a pure orthorhombic phase at a pressure of 0.4 GPa (Stage II, Figure 2B). The orthorhombic phase remained stable up to a pressure of 5.1 GPa. Increasing above this pressure, three neighboring peaks of the orthorhombic phase (i.e., (112), (020), and (200)) merged into one single, broad peak, indicating an amorphous-like phase (Figure 2C).[3,4,8] This pressure-induced amorphization included an intermediate phase, as shown by short-range, tetragonal ordering (Figure 2C). A similar orthorhombic-to-tetragonal phase transformation was observed in a thermally treated, single crystal of $CsPbBr_3$ perovskite. We refer to this local tetragonal-ordered amorphous phase as a "quasi-amorphous" phase (Stage III), which remained stable up to the peak pressure of 17.5 GPa (Figures 2A and Figure S5, Supporting Information). Upon release of pressure, the quasi-amorphous phase remained rigid, and, at pressure close to 0 GPa, it rapidly transformed to a single cubic phase (Stage IV) (Figures 2D and Figure S6, Supporting Information). Thus, it is suggested that the direct crystallization of perovskites from an amorphous precursor could cause the nucleation and growth of a single cubic perovskite phase.

Atomic movements that occur during phase transitions are important for the understanding and design of perovskite materials with precise structures and controlled properties.[9] We conducted a detailed, zoomed-in structural analysis in Stage II (see details in the Supporting Information). In this stage, the orthorhombic $CsPbBr_3$ NCs with the space group *Pnma* can be interpreted as a distorted perovskite structure in which the BX_6 units (i.e., $PbBr_6$ octahedra) are tilted compared to the cubic perovskite in the three-orthogonal Cartesian axial system (Figures S7 and S8, Supporting Information).[10] The tilting of the BX_6 octahedron

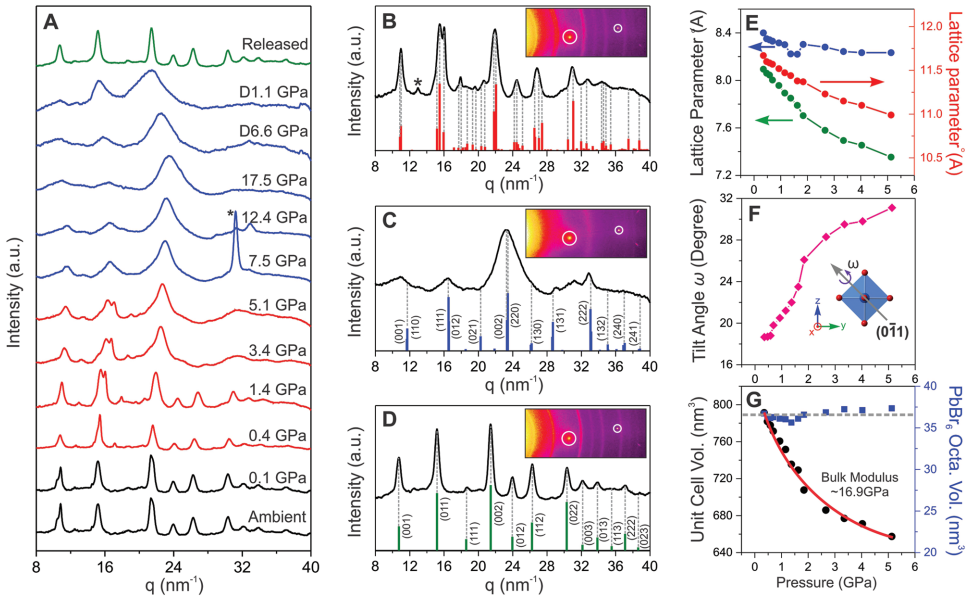

Figure 2. A) WAXS patterns during the compression and decompression processes. The WAXS patterns of different structural phases are coded by color, i.e., black for Stage I, red for Stage II, blue for Stage III, and green for Stage IV. A star labels the gasket peak. B–D) Integrated WAXS spectra with calculated Bragg reflection positions at 1.4, 14.5, and 0 GPa (after decompression), respectively. The bars show the calculated Bragg reflection positions of individual phases. The white circles in the insets are noise signals on the detector. E–G) Plots of the evolution of the structure as a function of pressure: E) orthorhombic perovskite lattice parameters (blue: *a*, red: *b*, green: *c*); F) the octahedral tilt angle; and G) the volumes of unit-cell (black) and $PbBr_6$ octahedron (blue). The red line in (G) is a fitted curve using the second-order Birch–Murnaghan equation of state, giving a bulk modulus of ≈16.9 GPa.

can be denoted by a Glazer notation of $a^-b^+a^-$ (Figure S8, Supporting Information) and described using a single tilt angle (ω) as long as the octahedra remain rigid (with all X-B-X angles being equal to 90°). Based on our structural assignments, the compression of lattice parameters (Figure 2E) indicated that the $PbBr_6$ octahedral tilt angle (ω) increased continuously from 18.7° at 0.4 GPa to 31.1° at 5.1 GPa in Stage II (Figure 2F and Figure S9 and Table S6, Supporting Information).[4a] Figure 2G shows the volumetric change of a unit cell as a function of pressure, which gives a bulk modulus of ≈16.9 GPa via fitting the second-order Birch–Murnaghan equation of state (see details in the Supporting Information).[11] The minimum variation of volume (1.4%) for the $PbBr_6$ octahedral units suggested that the octahedral tilting was wholly responsible for the reduction of the unit cell volume (Figure 2G). This result was consistent with the compressibility estimation calculated based on the bond-valence theory (see details in the Supporting Information), which showed exceptional rigidity of the $PbBr_6$ units (≈4.2 times more rigid than the $CsBr_{12}$ units; Table S1, Supporting Information).[12]

To further investigate the pressure-induced SL phase transformation at the mesoscale, we conducted a series of in situ SAXS measurements of the assembled NC-SLs.[13] **Figure 3**A,B shows typical SAXS patterns of the NC-SLs and the calculated *d*-spacings of SL(001) at various pressures, respectively. When the pressure was increased from 0 to 5 GPa, all of the SAXS peaks shifted to higher *q* positions, and, accordingly, the SL(001) *d*-spacing was reduced from 12.6 to 11.3 nm. Continuously increasing the pressure caused reversed shifts of both the SL(001) and inter-NC spacings. This change indicated that the NC-SL underwent a pressure-driven process

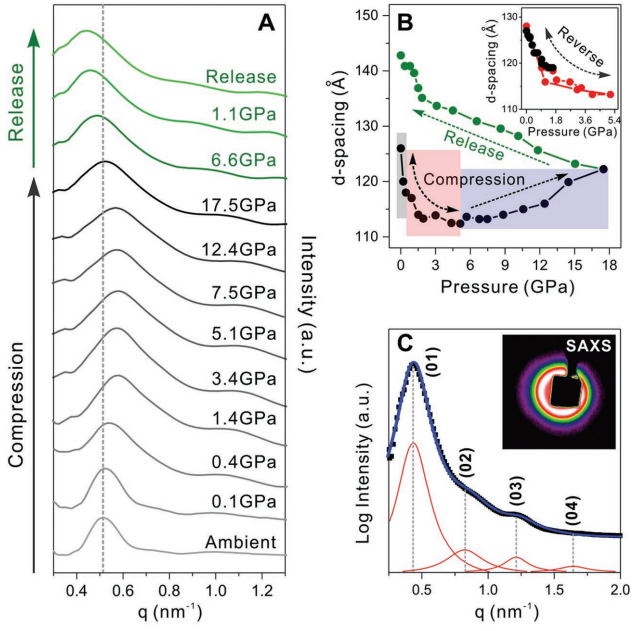

Figure 3. Superstructural evolution of the $CsPbBr_3$ perovskite NC-SLs under high pressure: A) in situ SAXS patterns; B) the corresponding SL(001) *d*-spacing of the first Bragg reflection of the SAXS spectra during compression (black, peak pressure of 17.5 GPa) and decompression (green) processes, showing a pressure-induced hysteresis. The inset in (B) shows the reversible change of *d*-spacing in the compression and release processes with a peak pressures of 1.3 GPa (black) and 5.1 GPa (red); C) SAXS pattern (integrated from the inset SAXS image) of the pressurized NC-SLs (peak pressure of 17.5 GPa). The fitted peaks shown in red present the sequence from (01) to (04) of the lamellar structure.

of detachment and rearrangement of surface ligands.[2b,14] Coincidentally, the reversal pressure of ≈5 GPa was close to the orthorhombic-to-quasi-amorphous transition pressure of 5.1 GPa. Thus, it is suggested that the atomic movement associated with phase transformation facilitated the detachment of ligands from the surfaces of NCs.[15] When the pressure was reduced to ambient pressure, the *d*-spacing of the SAXS peak did not return to 12.6 nm; instead, it continuously increased to 14.3 nm (Figure 3B). However, when the peak pressure was less than 5.1 GPa, irreversible *d*-spacing shift did not occur (Figure 3B, inset). The smearing of the SAXS patterns at high pressures did not allow for the determination of changes in the SL, but the recovered sample displayed a linear correlation, i.e., q/q_0 = 1/2/3/4 (Figure 3C and Table S7, Supporting Information), indicating the transformation of the SL phase from the initial simple cubic structure to the final lamellar SL structure.

Electron microscopy characterizations have provided evidence of the formation and preservation of pressure-driven lamellar SLs. The standing lamellar NPLs shown by TEM have uniform thicknesses of 10.1 ± 1.0 nm, which is equivalent to ≈17 atomic layers (**Figure 4**A, inset and Figure S14, Supporting Information).[16] TEM images of disassembled samples confirmed the formation of 2D, single-crystal NPLs with edge lengths of 20 to ≈100 nm (Figure 4A and Figure S15, Supporting Information). The HR-TEM images (Figure 4B and Figure S15, Supporting Information) and fast-Fourier transform (FFT) patterns (Figure 4B, inset) show a perfect single-crystalline cuboidal atomic lattice, consistent with the perfect cubic phase measured in WAXS (Figure 2D). The formation of irregularly shaped NPLs, such as concave NPLs, nanosquares, and nanoprisms (Figure 4A and Figure S16, Supporting Information), was also observed, suggesting that the formation of lateral NPLs resulted from pressure-driven, facet-to-facet attachment and the subsequent fusion of individual NCs.

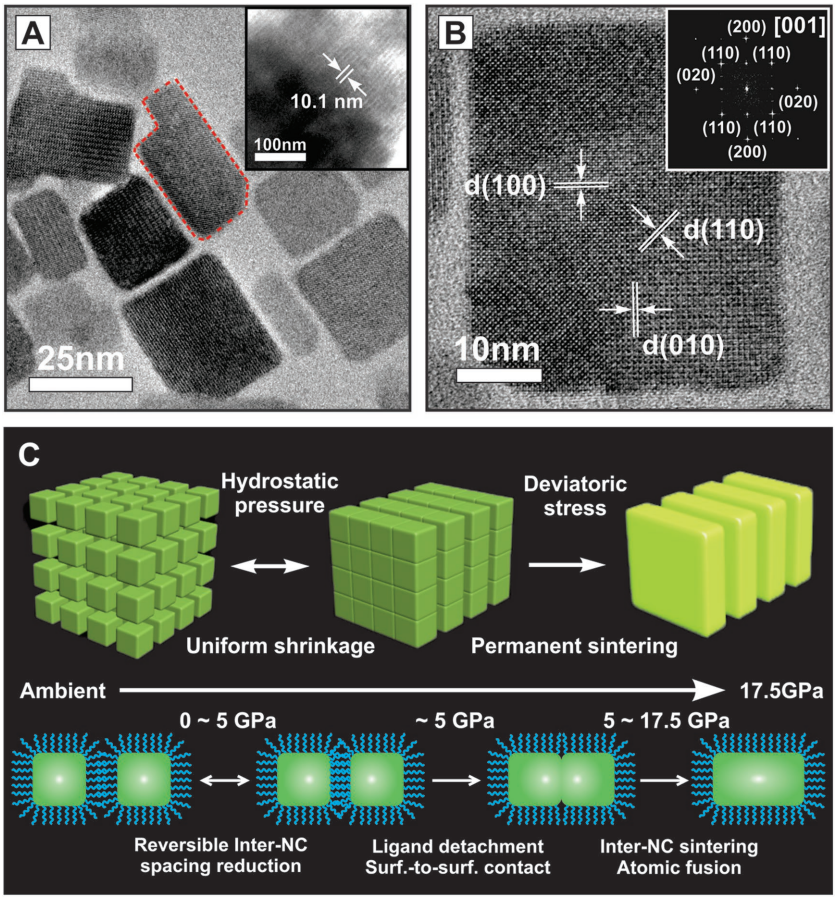

Figure 4. Formation of $CsPbBr_3$ perovskite NPLs under pressure: A) representative TEM image of the pressure-sintered NPLs. Inset: A TEM image of the pressurized sample with a lamellar structure before disassembly. B) An HR-TEM image and the corresponding FFT pattern (inset) of the pressure-synthesized $CsPbBr_3$ perovskite NPLs. C) Schematic demonstration of the proposed pressure-sintering process: NC-SL evolution (top) and interparticle fusion (bottom) under pressure. The particle labeled by the red dashed line in (A) shows a concave shape of NPL.

Analysis of the SAXS, WAXS, and TEM datasets allowed us to reconstruct the pressure-driven nucleation and growth pathway of large, 2D perovskite NPLs (Figure 4C). At pressures less than 5.1 GPa, the SLs are in a hydrostatic state in which the SLs shrink isotropically.[15] When the NC-SLs were compressed at pressures greater than 5.1 GPa, an anisotropic pressure gradient appeared across the SLs, initiating the deformation of organic ligands.[15] Increasing the pressure further ultimately drives the ligands to detach from the NCs. After the detached ligands migrate completely out of the gaps between the NCs, the NCs come into direct facet-to-facet contact and eventually fuse into 2D NPL (Figure 4C). The formation of large 2D NPLs also explains the stabilization of the single cubic phase by minimizing the surface area, thereby resulting in the dramatic release of the stress on the surface.[17]

In situ PL spectra were collected to evaluate the evolution of the band gaps in the $CsPbBr_3$ NCs associated with pressure-induced atomic and SL phase transformations (**Figure 5**A). The emission peak of the $CsPbBr_3$ NC-SLs shifted from 528 to 525 nm at 0.1 GPa, and the PL intensity was enhanced about sixfold (Figure 5B). While the small blueshift could be explained by the lattice compression,[2c] this dramatic enhancement of the PL intensity was most likely triggered by the reconstruction of the NC surfaces.[18] Upon further increase of pressure, a redshift in emissions and PL quenching occurred until the emission became undetectable at a pressure of 1.3 GPa (Figure 5A,B). This pressure-induced PL redshift has been reported in $MAPbX_3$ perovskites at a similar pressure region.[3,4] With further compression and decompression, no emissions associated with the NC-SLs were observed. However, returning the pressure to the ambient level caused reemergence of a green emission at 518 nm that was 1.6 times as intense as the emission of the starting perovskite NC-SLs. This emission increase was likely due to the formation of

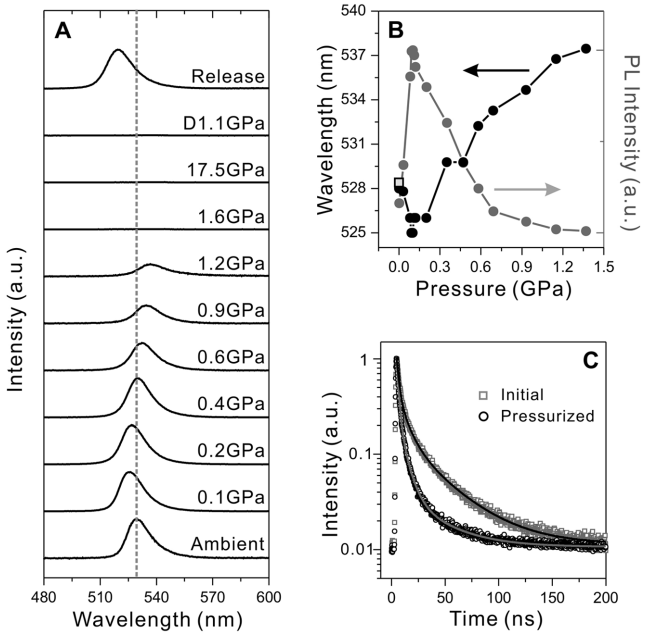

Figure 5. Optical properties of the $CsPbBr_3$ perovskite NCs under high-pressure: A) PL spectra of the evolution of the NC-SLs during the compression and decompression processes. B) Plots of the peak position of the NC-SL PLs (black) and the relative peak intensity (grey) as a function of the applied pressure. The square dot indicates the intensity of the PL peak of the NC-SLs after the pressure was released. C) Decay curves of the ensemble PL lifetime of the initial $CsPbBr_3$ perovskite NCs (black) and the final, pressure-synthesized $CsPbBr_3$ perovskite NPLs (grey). Exponentially fitted lines are shown in black and grey lines.

cubic perovskite NPLs (Stage IV) that have increased crystallinity and fewer defect and surface-related exciton trap states.[19] The two control experiments conducted at peak pressures of 1.3 and 5.1 GPa indicated that the emissions were recovered without any significant changes in the position and intensity of the PL (Figure S17, Supporting Information). This is consistent with that the NCs did not fuse into the 2D NPLs (Figure S18, Supporting Information) or have increased crystallinities (Figure S19, Supporting Information).

After the pressure-synthesized NPLs were dispersed in a toluene solution, their PL spectrum showed a symmetric emission peak at 504 nm with a narrow FWHM of ≈15 nm (Figure S20, Supporting Information). This suggested that the variously shaped NPLs with different lateral sizes had uniform thicknesses (quantum-confined dimension), consistent with our TEM measurements (Figure 4A and Figure S14, Supporting Information).[16] This further supports our proposed mechanism for the formation of NPLs from NCs (Figure 4C). The steady-state ensemble PL lifetime measurements of the NPLs (Figure 5C) showed long-lived charge carriers with a slow PL decay curve. The measured average lifetime of ≈23.6 ns was almost double the lifetime of the initial NCs (Figure 5C and Table S2, Supporting Information) and also dramatically longer than that of the $CsPbBr_3$ bulk materials.[20] In addition to the pressure-induced surface reconstruction, the PL enhancement and their longer lifetime also explained the single-crystallinity phase with minimal defects of the pressure-synthesized NPLs that had a low probability of recombination of the photogenerated electron and hole.[19b]

In conclusion, we probed the pressure-induced structural changes and property improvements of $CsPbBr_3$ NC-assembled SLs upon compression to 17.5 GPa. The $CsPbBr_3$ NCs underwent structural transitions from a mixture of cubic and orthorhombic phases, to a single orthorhombic phase (at 0.4 GPa), followed by a quasi-amorphous phase (at 5.1 GPa). During the processes, the SLs transformed from a simple cubic to a lamellar structure. Associated with the structural changes, the PL of the NC-SLs displayed a small pressure-induced blueshift and a sixfold enhancement in intensity at a pressure of 0.1 GPa, followed by a reversed redshift with a gradual decrease in intensity until it became undetectable at ≈1.3 GPa. Additionally, 2D lateral NPLs with a perfect cubic phase were formed through a pressure-gradient-induced inter-NC fusion process. The resultant NPLs not only have an increased crystallinity and uniform thicknesses, but also display an ≈1.6 time enhancement of PL intensity with a prolonged ensemble lifetime compared to the initial $CsPbBr_3$ NCs. The results presented here provide a new approach for combining nanocrystal assembly with pressure processing to make functional materials that have increased crystallinity, structural stability, and enhanced properties for applications in various technologies such as light emitting diodes and solar devices.

Supporting Information

Supporting Information is available from the Wiley Online Library or from the author.

Acknowledgements

O.C. acknowledges the support from the Brown University startup fund and the Salomon award fund. K.H. was supported by the GAANN research fellowship. CHESS was supported by the NSF award DMR-1332208. The authors thank Prof. Nitin Padture and Prof. Yuanyuan Zhou for valuable discussions about the manuscript. The TEM mesurements were performed at the Electron Microscopy Facility in the Institute for Molecular and Nanoscale Innovation (IMNI) at the Brown University.

Received: December 8, 2016
Revised: January 29, 2017
Published online:

[1] a) K. Gesi, K. Ozawa, S. Hirotsu, *J. Phys. Soc. Jpn.* **1975**, *38*, 463; b) Y. Kutes, L. H. Ye, Y. Y. Zhou, S. P. Pang, B. D. Huey, N. P. Padture, *J. Phys. Chem. Lett.* **2014**, *5*, 3335; c) A. Nurmikko, *Nat. Nanotechnol.* **2015**, *10*, 1001; d) H. Cho, S.-H. Jeong, M.-H. Park, Y.-H. Kim, C. Wolf, C.-L. Lee, J. H. Heo, A. Sadhanala, N. Myoung, S. Yoo, S. H. Im, R. H. Friend, T.-W. Lee, *Science* **2015**, *350*, 1222; e) A. Swarnkar, A. R. Marshall, E. M. Sanehira, B. D. Chernomordik, D. T. Moore, J. A. Christians, T. Chakrabarti, J. M. Luther, *Science* **2016**, *354*, 92; f) J. Byun, H. Cho, C. Wolf, M. Jang, A. Sadhanala, R. H. Friend, H. Yang, T.-W. Lee, *Adv. Mater.* **2016**, *28*, 7515; g) Y.-H. Kim, H. Cho, T.-W. Lee, *Proc. Natl. Acad. Sci. USA* **2016**, *113*, 11694.

[2] a) S. H. Tolbert, A. P. Alivisatos, *Science* **1994**, *265*, 373; b) Z. Wang, C. Schliehe, T. Wang, Y. Nagaoka, Y. C. Cao, W. A. Bassett, H. Wu, H. Fan, H. Weller, *J. Am. Chem. Soc.* **2011**, *133*, 14484;

c) S. H. Tolbert, A. P. Alivisatos, *J. Chem. Phys.* **1995**, *102*, 4642.
[3] Y. Wang, X. Lü, W. Yang, T. Wen, L. Yang, X. Ren, L. Wang, Z. Lin, Y. Zhao, *J. Am. Chem. Soc.* **2015**, *137*, 11144.
[4] a) S. Jiang, Y. Fang, R. Li, H. Xiao, J. Crowley, C. Wang, T. J. White, W. A. Goddard, Z. Wang, T. Baikie, J. Fang, *Angew. Chem., Int. Ed.* **2016**, *55*, 6540; b) L. Wang, K. Wang, G. Xiao, Q. Zeng, B. Zou, *J. Phys. Chem. Lett.* **2016**, *7*, 5273; c) L. Kong, G. Liu, J. Gong, Q. Hu, R. D. Schaller, P. Dera, D. Zhang, Z. Liu, W. Yang, K. Zhu, Y. Tang, C. Wang, S.-H. Wei, T. Xu, H.-K. Mao, *Proc. Natl. Acad. Sci. USA* **2016**, *113*, 8910.
[5] L. Protesescu, S. Yakunin, M. I. Bodnarchuk, F. Krieg, R. Caputo, C. H. Hendon, R. X. Yang, A. Walsh, M. V. Kovalenko, *Nano Lett.* **2015**, *15*, 3692.
[6] P. Cottingham, R. L. Brutchey, *Chem. Commun.* **2016**, *52*, 5246.
[7] B. O. Dabbousi, C. B. Murray, M. F. Rubner, M. G. Bawendi, *Chem. Mater.* **1994**, *6*, 216.
[8] a) I. P. Swainson, M. G. Tucker, D. J. Wilson, B. Winkler, V. Milman, *Chem. Mater.* **2007**, *19*, 2401; b) X. Lu, Y. Wang, C. C. Stoumpos, Q. Hu, X. Guo, H. Chen, L. Yang, J. S. Smith, W. Yang, Y. Zhao, H. Xu, M. G. Kanatzidis, Q. Jia, *Adv. Mater.* **2016**, *28*, 8663.
[9] M. J. Pitcher, P. Mandal, M. S. Dyer, J. Alaria, P. Borisov, H. Niu, J. B. Claridge, M. J. Rosseinsky, *Science* **2015**, *347*, 420.
[10] P. M. Lufaso, M. W. Woodward, *Acta Crystallogr., Sect. B: Struct. Sci.* **2001**, *857*, 725.
[11] a) Y. H. Chang, C. H. Park, K. Matsuishi, *J. Korean Phys. Soc.* **2004**, *44*, 889; b) P. Podsiadlo, B. Lee, V. B. Prakapenka, G. V. Krylova, R. D. Schaller, A. Demortiere, E. V. Shevchenko, *Nano Lett.* **2011**, *11*, 579.
[12] J. Zhao, N. L. Ross, D. Wang, R. J. Angel, *Acta Crystallogr., Sect. B: Struct. Sci.* **2004**, *60*, 263.
[13] Z. Wang, O. Chen, C. Y. Cao, K. Finkelstein, D.-M. Smilgies, X. Lu, W. A. Bassett, *Rev. Sci. Instrum.* **2010**, *81*, 093902.
[14] Z. Wang, X. D. Wen, R. Hoffmann, J. S. Son, R. Li, C. C. Fang, D. M. Smilgies, T. Hyeon, *Proc. Natl. Acad. Sci. USA* **2010**, *107*, 17119.
[15] a) T. Wang, R. Li, Z. Quan, W. S. Loc, W. A. Bassett, H. Xu, Y. C. Cao, J. Fang, Z. Wang, *Adv. Mater.* **2015**, *27*, 4544; b) H. Wu, F. Bai, Z. Sun, R. E. Haddad, D. M. Boye, Z. Wang, H. Fan, *Angew. Chem., Int. Ed.* **2010**, *49*, 8431.
[16] Y. Bekenstein, B. A. Koscher, S. W. Eaton, P. Yang, A. P. Alivisatos, *J. Am. Chem. Soc.* **2015**, *137*, 16008.
[17] J. Zhu, Z. Quan, C. Wang, X. Wen, Y. Jiang, J. Fang, Z. Wang, Y. Zhao, H. Xu, *Nanoscale* **2016**, *8*, 5214.
[18] a) M. A. Boles, D. Ling, T. Hyeon, D. V. Talapin, *Nat. Mater.* **2016**, *15*, 141; b) O. Chen, Y. Yang, T. Wang, H. Wu, C. Niu, J. Yang, Y. C. Cao, *J. Am. Chem. Soc.* **2011**, *133*, 17504.
[19] a) J. S. Manser, M. I. Saidaminov, J. A. Christians, O. M. Bakr, P. V. Kamat, *Acc. Chem. Res.* **2016**, *49*, 330; b) Y. X. Tian, A. Merdasa, E. Unger, M. Abdellah, K. B. Zheng, S. McKibbin, A. Mikkelsen, T. Pullerits, A. Yartsev, V. Sundstrom, I. G. Scheblykin, *J. Phys. Chem. Lett.* **2015**, *6*, 4171.
[20] N. Yantara, S. Bhaumik, F. Yan, D. Sabba, H. A. Dewi, N. Mathews, P. P. Boix, H. V. Demir, S. Mhaisalkar, *J. Phys. Chem. Lett.* **2015**, *6*, 4360.